Atmos. Chem. Phys. Discuss., 14, 17439–17478, 2014
www.atmos-chem-phys-discuss.net/14/17439/2014/
doi:10.5194/acpd-14-17439-2014

Atmospheric Chemistry and Physics
Discussions
Open Access

Evolution of aerosol chemistry in Xi'an, inland China during the dust storm period of 2013 – Part 1: Sources, chemical forms and formation mechanisms of nitrate and sulfate

G. H. Wang[1,2], Y. Huang[1,3], J. Tao[4], Y. Q. Ren[1,3], F. Wu[1], C. L. Cheng[1,3], J. J. Meng[1,3], J. J. Li[1], Y. T. Cheng[1,3], J. J. Cao[1], S. X. Liu[1], T. Zhang[1], and R. Zhang[1]

[1]State Key Laboratory of Loess and Quaternary Geology, Institute of Earth Environment, Chinese Academy of Sciences, Xi'an 710075, China
[2]School of Human Settlements and Civil Engineering, Xi'an Jiaotong University, Xi'an 710079, China
[3]University of Chinese Academy of Sciences, Beijing 100049, China
[4]South China Institute of Environmental Science, Guangzhou 510655, China

Received: 9 May 2014 – Accepted: 20 June 2014 – Published: 30 June 2014

Correspondence to: G. H. Wang (wanggh@ieecas.cn)

Published by Copernicus Publications on behalf of the European Geosciences Union.

Abstract

In the current work TSP sample was hourly collected in Xi'an, an inland mega-city of China near the Loess Plateau, during a dust storm event of 2013 (9 March 18:00–12 March 10:00 LT), along with a size-resolved aerosol sampling and an online measurement of $PM_{2.5}$. The TSP and size-resolved samples were determined for EC, OC, water-soluble organic carbon (WSOC) and nitrogen (WSON), inorganic ions and elements to investigate aerosol chemistry evolution. Hourly concentrations of Cl^-, NO_3^-, SO_4^{2-}, Na^+ and Ca^{2+} in the TSP samples reached up to 34, 12, 180, 72 and 28 µg m^{-3}, respectively, when dust peak arrived over Xi'an. Chemical compositions of the TSP samples showed that NH_4^+ and NO_3^- strongly correlated each other in the whole observation period ($r^2 = 0.76$), while SO_4^{2-} and Cl^- well correlated with Na^+, Ca^{2+}, Mg^{2+} and K^+ ($r^2 > 0.85$). Size distributions of NH_4^+ and NO_3^- presented a same pattern, which dominated in the coarse mode (> 2.1 µm) during the event and predominated in the fine mode (< 2.1 µm) during the non-event. SO_4^{2-} and Cl^- also dominated in the coarse mode during the event, but both exhibited two equivalent peaks in the fine and coarse modes during the non-event, respectively, due to the fine mode accumulations of secondarily produced SO_4^{2-} and biomass burning emitted Cl^- and the coarse mode enrichments of urban soil-derived SO_4^{2-} and Cl^-. Linear fit regression analysis further indicated that SO_4^{2-} and Cl^- in the dust samples possibly exist as Na_2SO_4, $CaSO_4$ and NaCl, which directly originated from Gobi desert surface soil, while NH_4^+ and NO_3^- in the dust samples exist as NH_4NO_3. We propose a mechanism to explain these observations in which aqueous phase of dust particle surface is formed via uptake of water vapor by hygroscopic Na_2SO_4, $CaSO_4$ and NaCl, followed by heterogeneous formation of nitrate on the liquid phase and subsequent absorption of ammonia. Our data indicate that 54 ± 20 % and 60 ± 23 % of NH_4^+ and NO_3^- during the dust period were secondarily produced via this pathway with the remaining derived from Gobi desert and Loess Plateau while SO_4^{2-} in the event almost entirely originated from the source

regions. To the best of our knowledge, the current work for the first time revealed an infant state of dust ageing process in the regions near the source, which is helpful for researchers to understand the panorama of dust ageing process from the source area to the downwind region.

1 Introduction

Mineral dust is the largest contributor to particulate matter in the atmosphere with estimated annual emission fluxes of 1000–3000 Tg (average, 1840 Tg) at present day (Dentener et al., 1996, 2006; Ginoux et al., 2001). Dust particles can influence the solar radiation directly by scattering sunlight and indirectly by acting as cloud condensation nuclei (CCN) and ice nuclei (IN) (Buseck and Pósfai, 1999; Formenti et al., 2011; Manktelow et al., 2010; Press, 2012). Gobi deserts of northern China and Mongolia and the Taklimakan desert of western China are the major source regions of East Asian dust (McNaughton et al., 2009; Mochida et al., 2007). Modeling results indicate that around 100–460 $\mathrm{Tg\,yr^{-1}}$ of dust is emitted annually from the East Asia source regions (Laura et al., 2006) and transport eastwardly, exerting a significant impact on the atmosphere over the downwind regions including east coastal China (Arimoto et al., 2006; Kim et al., 2004; Li et al., 2014; Li and Shao, 2009; Sun et al., 2010; Wang et al., 2012, 2013), Korea (Geng et al., 2014; Song et al., 2013; Sullivian et al., 2007), Japan (Takahashi et al., 2011; Tobo et al., 2010; Uno et al., 2009), and western America (Huebert et al., 2003; Leaitch et al., 2009; McNaughton et al., 2009; Parrington et al., 1983; Singh et al., 2009). A recent study found that dust from Sahara and Asia transport over Pacific Ocean and increase the snow precipitation in mountainous areas of Nevada, USA (Creamean et al., 2013). In addition to the impact on climate, dust storm also affect marine productivity because dust-bonded iron, nitrogen and phosphorus are the important nutrients to marine microbes (Boyd et al., 2007; Duce et al., 2008; Jickells et al., 2005; Kanakidou et al., 2012; Zamora et al., 2011, 2013).

Due to rapid urbanization and industrialization in China, annual consumption of coal has increased to 3.61 billiontons in the country recently (China Statistic Press, 2010), along with a sharp increase in vehicle numbers, resulting in high burden of SO_2, NO_x, EC, nitrate, sulfate, and other pollutants in the atmosphere over China (Geng et al., 2014; He, 2014; Huang et al., 2014; van Donkelaar et al., 2010; Wang et al., 2014). During the long-range transport dust can become coated with nitrate, sulfate, ammonium and other pollutants, leading to a series of changes in dust behavior in the atmosphere such as water uptake, deposition, and scattering sunlight (Boreddy et al., 2014; Creamean et al., 2013; Formenti et al., 2011; Grassian, 2001; Seinfeld et al., 2004; Sullivan et al., 2009a). Studies found that SO_2 level in China has become stable and even decreased since 2006 because Chinese government has promulgated a strict standard on SO_2 emission (Lu et al., 2010; Menon et al., 2008; Wang et al., 2013). As a result, atmospheric sulfate aerosol loading has been decreasing in many Chinese urban regions since 2006, whereas NO_x and particulate nitrate levels have kept stable and even increase (Wang et al., 2011, 2012, 2013; Zhang et al., 2009). Due to the chemical affinity of nitrogen oxides and nitric acid with dust particles (Hanisch and Crowley, 2001; Mogili et al., 2006; Saliba and Chamseddine, 2012; Song et al., 2013; Usher et al., 2003), such a change in the atmospheric environment of China suggests that dust particle behavior might also be changing compared to the situations ten years ago. Therefore, it is necessary to investigate the present physicochemical properties of airborne particles in the country during dusty periods.

In the past decades, numerous observations have been conducted along the Asian dust transport pathways including east coastal China, Korea, Japan, Pacific Ocean and western America to investigate the ageing process of Asian dust during the transport (Huebert et al., 2003; Kim et al., 2004). On contrast, only a few field measurements have been done in the upstream regions especially inland cities of China (Arimoto et al., 2004; Huang et al., 2010), where the dust particle ageing could be at the infant state due to the proximity of the source regions including deserts and Loess Plateau. Xi’an is a mega-city in inland China, which is located at the south edge of Loess Plateau.

High level of particle pollution has been a persistent problem in the city. In comparison with that in 1997 the annual level of sulfate aerosol in the city in 2012 has decreased by a factor of two. On the other hand, however, NO_x and nitrate have increased about 25 %. Acidic gases concentration is a key factor affecting heterogeneous reaction rates of dust particle with SO_2, NO_x and HNO_3 (g), apart from relative humidity, temperature and dust mineralogy and morphology. For example, calcite ($CaCO_3$), which is a common component of East Asian dust and account for 10–30 % of the dust mass, can rapidly convert to $Ca(NO_3)_2$ less than 3 min under 1 ppbv HNO_3 but longer than 4 h under low HNO_3 mixing ratio (10 pptv) (Sullivan et al., 2009b). Since $Ca(NO_3)_2$ is highly hygroscopic, the chemically modified dust can absorb water vapor and form a liquid phase on the surface (Li et al., 2014). Therefore, changes in physicochemical properties of dust particles occur and are probably much more significant than before due to the recent increase in NO_x emission. In order to investigate the impact of dust storm on the downwind aerosol chemistry under the current high level of NO_x and relatively low level of SO_2 conditions, we performed an intensive filter-based sampling with a 1 h time resolution to investigate chemical evolution of urban airborne particles in Xi'an in the period of 9–12 March 2013, during which the annual heaviest dust storm passed through the city with an hourly maximum of TSP more than 7000 $\mu g\,m^{-3}$. In the current work, we focus on the changes in aerosol chemistry specifically nitrate and sulfate during the event. We first investigate the composition and size distribution of airborne particles in the event and compare with those in the non-event to discuss the chemical evolution of dust particles. Then we identify the chemical forms of nitrates and sulfates existing in the dust to explore their sources and formation mechanisms. We found for the first time an enrichment of ammonium nitrate in dust particles, which is different from a fine mode accumulation of ammonium sulfate in Asian dust continental outflow region. Our results further demonstrated that such a phenomenon is relevant to mineral dusts, which consist of hygroscopic salts (NaCl, Na_2SO_4 and $CaSO_4$) and originate from dried salt lakes in west and north parts of China and Gobi deserts.

2 Experimental section

2.1 Collections of TSP and size-resolved samples

TSP samples were hourly collected at an airflow rate of 1.0 $m^3 min^{-1}$ from 9 March 18:00–12 March 10:00 LT by using two air samplers TCH-1000 (Tianhong Company, China) on the rooftop of a three-story building on the campus of Institute of Earth Environment, CAS, which is located in the downtown area of Xi'an. Simultaneously, size-segregated samplers were also collected with each set lasting for 3 h during the dust storm period and 12 h during the non-dust event. The cutoff points of the size-segregated samples are 0.4, 0.7, 1.1, 2.1, 3.3, 4.7, 5.8 and 9.0 µm at an airflow rate of 28.3 $L min^{-1}$. All the samples were collected onto pre-combusted quartz filters (450 °C for 6 h). Field blank samplers were also collected at the beginning and the end of the sampling campaign by mounting pre-baked blank filters onto the samplers for about 10 min without sucking any air. After sampling, all the filters were individually sealed in aluminum foil bags and stored at −20 °C prior to analysis. A total of 65 TSP samples and six sets of size-segregated samples were collected. In addition to the above filter-based sampling, online measurement of $PM_{2.5}$ was also conducted by using E-BAM-9800 analyzer (Met One, USA).

2.2 Analyses of TSP and size-resolved samples

2.2.1 Inorganic ions, water-soluble organic (WSOC) and inorganic carbon (WSIC), and water-soluble organic nitrogen (WSON)

Aliquot (size: 12.56 cm^2) of the filter was cut into pieces and extracted for three times with Milli-Q pure water under sonication. One part of the combined water-extracts was determined for inorganic ions using Dionex-6000 ion chromatography. Another part of the water-extracts was determined for water-soluble organic carbon (WSOC), water-soluble inorganic carbon (WSIC) and water-soluble total nitrogen (WSTN) using Shimadzu 5000 TOC/N Analyzer. The detailed analysis methods for inorganic ions, WSOC and WSTN can be found elsewhere (Wang et al., 2010). NO_3^- and NH_4^+ are the major water-soluble inorganic nitrogen (WSIN) species in airborne particles, thus the difference between WSTN and WSIN is defined as water-soluble organic nitrogen (WSON).

2.2.2 Organic carbon (OC) and elemental carbon (EC)

OC and EC in the TSP samples were measured by a DRI Model 2001 Carbon Analyzer using the Interagency Monitoring of Protected Visual Environments (IMPROVE) thermal/optical reflectance (TOR) protocol. Briefly, a size of 0.53 cm^2 filter was put in a quartz boat inside the analyzer and progressively heated to temperatures of 120 °C, 250 °C, 450 °C, and 550 °C in a non-oxidizing helium (He) atmosphere, and 550 °C, 700 °C, and 800 °C in an oxidizing atmosphere containing 2 % oxygen in helium.

2.2.3 Elements

Elements of the TSP samples were determined by Energy Dispersive X-Ray Fluorescence (ED-XRF) spectrometry (Epsilon 5 ED-XRF, PANalytical B. V., Netherlands). The X-ray source is a side window X-ray tube with a gadolinium anode and operated at an accelerating voltage of 25e100 kV and a current of 0.5e24 mA (maximum power: 600 W). The characteristic X-ray radiation is detected by a germanium detector (PAN 32). Each sample was analyzed for 30 min to obtain a spectrum of X-ray counts vs. photon energy with the individual peak energies matching specific elements and peak areas corresponding to elemental concentrations. The spectrometer was calibrated with thin-film standards obtained from MicroMatter Co. (Arlington, WA, USA). In the current study, 14 elements (i.e., S, Cl, K, Ca, Ti, Mn, Fe, Zn, Cr, Ni, As, Br, Mo, Pb) were determined. The element concentrations for blank quartz fiber filter are 0.00–0.66 $\mu g\,cm^{-2}$ and lower than 10 % of those in the TSP samples.

3 Results and discussion

During the sampling period a massive dust storm event originating from Mongolia Gobi desert arrived over Xi'an on 9 March with a highest TSP level of 7527 µg m^{-3} at the beginning hour (18:00 LT) and a second peak at 10 March 13:00 LT. From 9 March 18:00 to 10 March 21:00 LT TSP level decreased from the highest to less than 1000 µg m^{-3} that is a typical level of TSP in X'an during spring. A 48 h backward trajectory analysis indicated a three-phase pattern for the movements of air masses arrived in Xi'an during the sampling period. As seen in Fig. 1, the 48 h backward trajectories showed that from 9 March 18:00 to 10 March 21:00 LT air parcels from Gobi deserts of Mongolia and North China directly transported to Xi'an at 100 m, 300 m and 500 m levels above the ground along the same tracks. TSP within this period ranged from 774–7527 µg m^{-3} with an average of 2109 ± 1360 µg m^{-3}. We classified this period as dust storm event (Phase I, see Fig. 1a and b for examples). From 10 March 21:00 to 11 March 12:00 LT air parcels at the 100 m and 300 m levels still originated from the Gobi deserts but moved to east coastal China first and then returned to Xi'an, while the 500 m air parcel originated from southern China and moved slowly to Xi'an after spanned over Qinling Mountain (Fig. 1c and e). During this period the TSP level ranged from 412 to 1037 µg m^{-3} with an average of 630 ± 155 µg m^{-3} (Table 1, hereinafter). We classified this period as transition period (Phase II, see Fig. 1c for example). After 11 March, 12:00 LT, the three levels of air parcels originated from North China Plain and moved to Xi'an from Qinling Mountain (about 1500 m above the ground level, Fig. 1d and e). During this period the TSP varied from 476–1399 µg m^{-3} with an average of 687 ± 194 µg m^{-3}. We classified this period as non-dust storm period (Phase III, see Fig. 1d for example). As seen in Fig. 1e, Xi'an is located in Guanzhong Basin and very close to Qinling Mountain. From the transport tracks it can be seen that air parcels within the Phase III moved slowly in comparison with those in Phase I and Phase II. Thus, we believe that aerosols in the non-dust storm period are mostly derived from the local sources rather than long range transport. In the following sections we will discuss the aerosol chemistry evolution based on the three classified categories.

3.1 Hourly changes in chemical compositions of ambient particles

As shown in Fig. 2a, during the dust storm period TSP showed two maxima with the largest peak at the first hour (i.e., 9 March, 18:00 LT) and a second peak at the noon time (10 March, 11:00–13:00 LT) of 10 March. At the same time $PM_{2.5}$ was $152 \pm 127\,\mu g\,m^{-3}$ with a maximum of $621\,\mu g\,m^{-3}$ occurring at the first hour (Fig. 2a). As shown Table 1, relative abundances of $PM_{2.5}$/TSP were $7.4 \pm 3.4\,\%$, $14 \pm 2.3\,\%$, and $23 \pm 4.8\,\%$ during the dust storm event, transition period and non-dust storm event, respectively, suggesting that surface soils in Gobi deserts and Loess Plateau consist of a certain amount of fine particles. From the backward trajectories we found that air parcels at the first ten hours directly moved across the Guanzhong Basin from the north to the south (as exemplified in Fig. 1a), sweeping pollutants out of Xi'an. Then, the air mass moved to Xi'an from the east at 10 March 10:00 LT (see Fig. 1b for an example) with pollutants originating from the upwind cities such as Weinan and Huayin. As a result, EC was almost undetectable at the beginning ten hours but sharply increased to more than $30\,\mu g\,m^{-3}$ at the 10 March noon time during the dust storm period (Fig. 2b).

Total inorganic ions in the dust storm, transition and non-dust storm periods accounted for 4, 8 and 12 % of the TSP mass, respectively (Fig. 3). In contrast, relative abundance of WSOC to OC at the three periods gradually decreased from 0.4 in the dust period to 0.3 in the non-dust period (Fig. 3), which is lower than that (0.5 ± 0.1) observed for dust storm events in the spring of 2009 (Wang et al., 2013). Our previous studies found that dusts from Gobi deserts contain significant amounts of water-soluble organic compounds, e.g., trehalose (Wang et al., 2011, 2012). In addition, heterogeneous formation of SOA on dust surface is another important contributor to WSOC of dust (Sullivan and Prather, 2007; Wang et al., 2013). Therefore, in comparison with that in 2009 spring the lower ratio of WSOC/OC is most likely due to the differences in the dust source regions and/or SOA formation on the dust surface. OC/EC ratio presented similar values during the transition and non-dust periods with an average value around 4.0, which is higher than that for $PM_{2.5}$ in the city since coarse particles contain less amount of elemental carbon. Our previous investigation on impact of Asian dust storm on Xi'an aerosols in the spring of 2009 found that 88 % (in mass) of airborne particulate sulfate originates from Gobi desert soil in the presence of dust storm (Wang et al., 2011, 2013). A recent study on the atmospheric aerosols collected in Taklimakan desert also found that airborne particles in the desert are abundant in sulfate, which accounts for about 4 % the particle mass with no significant difference for particles with different sizes (Wu et al., 2012). WSOC/WSON ratios are higher in the dust storm and transition periods and lower in the non-dust period, which can be ascribed to more WSON species emitted from anthropogenic species such as urea and amines (Cape et al., 2011; Chen et al., 2010; Wang et al., 2010).

As shown in Fig. 4a, extremely high levels of sulfate were observed during the dust storm period (Phase I) with a peak of 180 $\mu g\,m^{-3}$ at the first hour, accounting for 2.3 % of the TSP mass (Table 1), which falls in the range reported for the airborne dust in Taklimakan desert by Wu et al. (2012). Due to the second peak of dust storm arrived in Xi'an at the noon of 10 March, sulfate showed a moderate peak as did TSP (see the inserted figure in Fig. 4a). During the whole sampling period nitrate and ammonium displayed similar variation patterns, which are different from other ions and are almost continuously increasing from the dust storm period to the non-dust storm period (Fig. 4b). Temporal variation pattern of Cl^- is similar to that of SO_4^{2-} while the variation pattern of F^- is similar to EC, indicating that Cl^- and SO_4^{2-} are of similar natural origins but F^- and EC are of common anthropogenic sources, e.g., coal combustion (Wang et al., 2010). There are many dried salt lakes in north and west parts of China and Gobi area of Mongolia, in which halite (NaCl), gypsum ($CaSO_4$), mirabilite (Na_2SO_4) and other salts are common components of the surface soil (Zheng, 1991). Mineral species containing calcium and magnesium often co-exist in desert regions. For example, dolomite ($CaMg(CO_3)_2$) is a common mineral salt in surface soil in Taklimakan, Gobi desert and Loess Plateau of China (Li et al., 2007; Maher et al., 2009). Thus, both presented the same temporal pattern during the dust and transition periods when dust particles from the above region are dominant (Fig. 4d). However, Ca^{2+} and Mg^{2+} displayed divergent patterns in the non-dust storm period when the aerosols are dominated by local sources, indicating both ions are of different origins.

As seen in Fig. 5a, relative abundance of elemental calcium to TSP (Ca/TSP) during the whole sampling period was nearly constant, which slightly increased from 6.9 ± 1.0 % in the event to 8.2 ± 1.4 % in the non-event. In contrast, ratio of Ca^{2+}/Ca was keeping increase from 7.1 ± 2.8 % in the event, 16 ± 6.0 % in the transition period to 22 ± 5.7 % in the non-event, indicating an enrichment of local soil that consists of more water-soluble calcium and/or a continuous conversion of elemental calcium into calcium cation. Although the mass ratio of SO_4^{2-}/TSP displayed an increasing trend from about 1.0 % during the dust storm event to about 5.0 % in the non-event, the ratios of SO_4^{2-}-S/total-S in the TSP samples during the three periods are almost the same (Fig. 5b), which are 62 ± 13 % in the dust storm event, 61 ± 6.1 % in the transition time, and 54 ± 5.2 %, in the non-event period, respectively, suggesting that sulfate in the samples is largely derived from dust/soil and photochemical production of sulfate was minor even in the non-dust period. Such a result is consistent with the observation for the dust particles during the spring of 2009, by which we found only 12 % of particulate sulfate in Xi'an at that time was formed by heterogeneous formation and 88 % of the sulfate was transported from the desert region (Wang et al., 2013).

3.2 Size distributions

Size is an important parameter of an aerosol, which is related to its origin, formation pathway and composition (Hinds, 1999). To further investigate the chemical evolution process of the urban aerosols, size-resolved chemical compositions were analyzed for the dust storm and non-dust storm periods. The size-segregated samples collected in the transition period were not used in this study because sampling duration of these samples overlapped somewhat with the non-dust period. As shown in Fig. 6a, Cl^- presented a bimodal pattern in the dust storm period with a large peak in the coarse mode (> 2.1 µm) and a small peak in the fine mode (< 2.1 µm), in contrast to the case in the non-dust storm period, which is characterized by two equivalent peaks in the fine and coarse modes, respectively. The pronounced coarse mode peak in the dust storm period further suggests the origins of NaCl$^-$ from dried salt lakes in the Gobi desert region. Nitrate and sulfate dominated in the coarse mode when dust was present, but nitrate in the fine mode was much more abundant than in the coarse mode in the non-dust storm period while sulfate displayed two equivalent peaks in both modes (Fig. 6b and c). The sulfate distribution patterns in the dust storm and non-dust storm periods are similar to those of Cl$^-$, while nitrate displayed similar patterns to those of ammonium in both periods (Fig. 6b–d). During the non-dust storm period Cl$^-$, NO_3^- and SO_4^{2-} in the fine mode (< 2.1 µm) accounted for 55, 58 and 54 % of the mass in the whole size range, respectively (Table 2). Whereas in the dust event the fine modes of Cl$^-$, NO_3^- and SO_4^{2-} decreased significantly, accounting for 40 ± 4 %, 31 ± 6 % and 27 ± 7 % of the total, respectively (Table 2).

Size distribution patterns of Na$^+$ are almost identical with those of Cl$^-$ in both dust and non-dust storm periods (Fig. 6a and e), indicating that both have the same sources even in the non-dust storm period. K$^+$ is a tracer of biomass burning smoke and enriched in fine particles, thus the fine mode (< 2.1 µm) of K$^+$ was relatively low in the dust storm period, accounting for 40 ± 7 % of the total mass in the whole size range, and became predominant in the non-dust storm period, accounting for 66 % of the total (Fig. 6f and Table 2). Since Mg^{2+} and Ca^{2+} are largely derived from soil, both dominated in the coarse mode during the dust and non-dust periods (Fig. 6g and h).

3.3 Chemical forms, sources and productions of nitrate and sulfate

Figure 7 shows the linear fit regressions for nitrate, sulfate, ammonium and other major cations in the TSP samples during the dust storm and transition periods. Nitrate showed a robust correlation with ammonium ($r^2 = 0.76$, Fig. 7a) but presented no correlation with the sum of Na$^+$, K$^+$, Mg^{2+} plus Ca^{2+} (Fig. 7b). On the contrary, sulfate during the dust storm and transition periods did not correlate with ammonium but strongly correlated with the sum of the cations (Fig. 7c and d). Interestingly, robust linear correlations ($R^2 > 0.99$) were found for the samples collected at the beginning three hours (red dots in Fig. 7a–d), suggesting that dust particles in the city within this period are of the same chemical compositions and are not chemically modified. Since nitrate and ammonium displayed the same size distribution patterns during the whole sampling period, the strong linear correlation between nitrate and ammonium with a slope of 0.28 suggests that NH_4NO_3 is the major chemical form of both ions in the airborne particles, especially in the dust storm and transition periods. Equivalent percentages showed that Na^+ and Ca^{2+} are the two major cations during the dust storm and transition periods, accounting for 77 ± 5.0 % (range, 65–87 %) of the total cation equivalent (Fig. 8a). Nitrate and sulfate are the two major anions, accounting for 86 ± 2.1 % (range, 80–90 %) of the total anion equivalent (Fig. 8b). As discussed above, NaCl and NH_4NO_3 are the major chemical forms of Cl^- and NO_3^- in the TSP samples, respectively. Thus, it is reasonably expected that the remaining Na^+ and other major cations in the samples exist as sulfate salts (i.e., Na_2SO_4, $CaSO_4$, $MgSO_4$ and K_2SO_4) during the dust storm and transition periods. Concentrations of these sulfate salts during the dust and transition periods and their relative abundances to the total sulfate in the water-soluble fraction are summarized in Table 3 and shown in Fig. 9. Within these periods Na_2SO_4 and $CaSO_4$ are the major sulfate salts, which originate from dust source regions and account for more than 90 % of the total water-soluble sulfate salts.

Figure 10a shows a temporal variation in molar ratio of NO_3^- to SO_4^{2-} during the whole period. Because nitrate in Gobi desert surface soil is much less than sulfate, the molar ratio of $NO_3^-$to SO_4^{2-} at the beginning hours was very low and gradually increased along with an increase in the observation time, indicating that the heterogeneous formation of NO_3^- on dust surface is faster than SO_4^{2-}. For example, during the nighttime of 9 and 10 molar ratio of NO_3^-/SO_4^{2-} increased by a rate of 0.07 h^{-1} (Fig. 10b). As discussed above dust particles at the first three hours during the dust storm period were not chemically modified, and EC at that time was zero. Thus, here we use the first sample as a reference to calculate the heterogeneous productions of NO_3^-, SO_4^{2-} and NH_4^+ for the remaining TSP samples by using the following equation.

$$\mathrm{d}A = C_A^i - \frac{C_A^{\mathrm{ref}}}{C_{\mathrm{TSP}}^{\mathrm{ref}}} \cdot C_{\mathrm{TSP}}^i$$

Where dA is the secondarily formed NO_3^-, SO_4^{2-} or NH_4^+ in the sample i, C_A^i is the concentration of NO_3^-, SO_4^{2-} or NH_4^+ in the sample i, C_A^{ref} is the concentration of NO_3^-, SO_4^{2-} or NH_4^+ in the first sample at the beginning hour of the dust storm period, $C_{\mathrm{TSP}}^{\mathrm{ref}}$ is the TSP concentration of the first sample, and C_{TSP}^i is the TSP concentration of the sample i.

The calculated results, i.e., dNO_3^-, dSO_4^{2-} and dNH_4^+, are produced by heterogeneous reactions of HNO_3(g), NO_x, SO_2 and NH_3 on the dust surface and are normalized by the total. As seen in Fig. 11, dNO_3^-/total-NO_3^- and dNH_4^+/total-NH_4^+ presented identical variation patterns with a sharp increase from less than 0.1 to 0.9 in the dust storm and transition periods and then to above 0.9 in the non-dust period. However, the ratio of dSO_4^{2-}/total-SO_4^{2-} is almost zero in the dust storm and transition periods and increased to about 0.4 at the late hours of the non-dust storm period. Such phenomena again demonstrate that nitrate and ammonium in the airborne particles during the whole campaign existed as the chemical form of NH_4NO_3 and its production speed is much faster than sulfate. In the dust storm period SO_4^{2-} almost entirely originated from surface soil in Gobi desert and no significant amount of SO_4^{2-} in the dust storm event was secondarily produced (Fig. 11). Here, we propose a three-step mechanism of heterogeneous formation of nitrate on dust surface to explain the formation of NH_4NO_3 (see Fig. 12). As discussed above, the airborne particles during the dust storm and transition period consist of significant amounts of water-soluble NaCl, Na_2SO_4 and $CaSO_4$. These compounds are very hygroscopic and thus can take up water vapor, forming a liquid phase on the dust surface even under the low RH conditions of the dust storm period (RH = 14–26 %, Table 1). The aqueous phase is favorable for the formation of NH_4NO_3, which is probably formed via a gas-phase homogeneous reaction of nitric acid with ammonia and a subsequent partitioning into the liquid phase (Nie et al., 2012; Pathak et al., 2011). In addition, NO_3^- can also be produced in the liquid phase via heterogeneous reactions of gaseous HNO_3, N_2O_5 and NO_x with dust particles (Finlayson-Pitts et al., 2003; Hanisch and Crowley, 2001; Laskin et al., 2005; Usher et al., 2003), followed by a subsequent absorption of the gas-phase NH_3 to form NH_4NO_3 (as illustrated by Fig. 12). As a result, an enrichment of NH_4^+ in the coarse mode (> 2.1 µm) was observed during the dust storm and transition period when dust particles were dominant (Fig. 6). These kinds of phenomena are different from the cases in the East Asia continental outflow region including north Pacific and west America (Fairlie et al., 2010; Sullivian et al., 2007), where in the presence of Asian dust ammonium is often enriched in fine particles as ammonium sulfate and/or ammonium bisulfate that is formed by heterogeneous reactions, although nitrate is still in coarse mode. Such differences indicate an infant state of chemical evolution of dust particles in Xi'an, wich is near the dust source regions.

4 Summary and conclusions

High time resolution of TSP and size-resolved samples in Xi'an, inland China during a dust episode occurring in the March of 2013 were collected and categorized as three groups, i.e., dust storm, transition and non-dust storm samples, based on the TSP levels and air parcel movement tracks. Nitrate in the TSP samples only showed a strong linear correlation with ammonium during the whole sampling period. On the contrary, sulfate and chloride well correlated with Na^+, Ca^{2+}, Mg^{2+} and K^+ but not correlated with ammonium especially in the dust storm and transition periods. Size distribution pattern of NO_3^- is similar to that of NH_4^+, which presented a bimodal pattern with a dominant peak in the coarse mode when dust storm occurred and with a predominant peak in the fine mode in the absence of dust storm. In the event size distribution patterns

Cl^- and SO_4^- are similar to Na^+, Ca^{2+}, Mg^{2+} and K^+, which dominated in the coarse mode. During the non-event Cl^-, SO_4^- and K^+ showed an increase in the fine mode due to enhancements of biomass burning emission and secondary oxidation. Based on the above correlations and size distribution pattern, we assumed that NO_3^-, SO_4^{2-} and Cl^- in the airborne particles during the whole campaign possibly existed as NH_4NO_3, Na_2SO_4, $CaSO_4$, $MgSO_4$, K_2SO_4 and NaCl. Molar ratio of NO_3^-/SO_4^{2-} was observed to continuously increase from less than 0.1 at the moment of the dust storm peak arrived in the city to about 2.5 during the non-dust storm event, demonstrating that nitrate production is much faster than sulfate. Secondarily produced NH_4^+ and NO_3^- accounted for 54 ± 20 % and 60 ± 23 % of the total in the dust storm period, 87 ± 4.0 % and 91 ± 3.0 % of the total in the transition period and 94 ± 2.0 % and 96 ± 1.0 % of the total in the non-dust storm period, respectively. On contrast, secondarily produced SO_4^{2-} is almost zero in the dust storm period and accounted for 5.0 ± 6.0 % of the total at the transition time and 21 ± 15 % of the total in the non-dust storm period. Sulfate in the dust storm period is almost entirely transported from Gobi desert surface soil as chemical forms of Na_2SO_4 and $CaSO_4$ that are common minerals in the desert region. Our observation results also indicate that in the presence of dust storm, particles that contain hygroscopic NaCl, Na_2SO_4 and $CaSO_4$ can take up water vapor and form a liquid phase on the particle surface, which results in the formation of nitrate and the subsequent absorption of ammonia to form NH_4NO_3. Therefore, a coarse mode of NH_4^+ was observed during the dust storm period. These phenomena not only demonstrate a faster production of nitrate than sulfate but also indicate an infant state of chemical evolution of dust particles in the regions near the source.

Acknowledgements. This work was financially supported by China National Science Funds for Distinguished Young Scholars (Grant N0. 41325014), and the “Strategic Priority Research Program” of the Chinese Academy of Sciences (Grant No. XDA05100103, XDB05020401).

References

Arimoto, R., Zhang, X. Y., Huebert, B. J., Kang, C. H., Savoie, D. L., Prospero, J. M., Sage, S. K., Schloesslin, C. A., Khaing, H. M., and Oh, S. N.: Chemical composition of atmospheric aerosols from Zhenbeitai, China, and Gosan, South Korea, during ACE-Asia, J. Geophys. Res.-Atmos., 109, D19S04, doi:10.1029/2003JD004323, 2004.

Arimoto, R., Kim, Y. J., Kim, Y. P., Quinn, P. K., Bates, T. S., Anderson, T. L., Gong, S., Uno, I., Chin, M., Huebert, B. J., Clarke, A. D., Shinozuka, Y., Weber, R. J., Anderson, J. R., Guazzotti, S. A., Sullivan, R. C., Sodeman, D. A., Prather, K. A., and Sokolik, I. N.: Characterization of Asian Dust during ACE-Asia, Global Planet. Change, 52, 23–56, 2006.

Boreddy, S. K. R., Kawamura, K., and Jung, J.: Hygroscopic properties of particles nebulized from water extracts of aerosols collected at Chichijima Island in the western North Pacific: an outflow region of Asian dust, J. Geophys. Res.-Atmos., 119, 167–178, doi:10.1002/2013JD020626, 2014.

Boyd, P. W., Jickells, T., Law, C. S., Blain, S., Boyle, E. A., Buesseler, K. O., Coale, K. H., Cullen, J. J., de Baar, H. J. W., Follows, M., Harvey, M., Lancelot, C., Levasseur, M., Owens, N. P. J., Pollard, R., Rivkin, R. B., Sarmiento, J., Schoemann, V., Smetacek, V., Takeda, S., Tsuda, A., Turner, S., and Watson, A. J.: Mesoscale Iron Enrichment Experiments 1993–2005: synthesis and future directions, Science, 315, 612–617, 2007.

Buseck, P. R. and Pósfai, M.: Airborne minerals and related aerosol particles: effects on climate and the environment, P. Natl. Acad. Sci. USA, 96, 3372–3379, 1999.

Cape, J. N., Cornell, S. E., Jickells, T. D., and Nemitz, E.: Organic nitrogen in the atmosphere – where does it come from? A review of sources and methods, Atmos. Res., 102, 30–48, 2011.

Chen, H. Y., Chen, L. D., Chiang, Z. Y., Hung, C. C., Lin, F. J., Chou, W. C., Gong, G. C., and Wen, L. S.: Size fractionation and molecular composition of water-soluble inorganic and organic nitrogen in aerosols of a coastal environment, J. Geophys. Res.-Atmos., 115, D22307, doi:10.1029/2010JD014157, 2010.

China Statistical Press: China Statistical Yearbook, edited, Chinese Statistics Press, Beijing, 2012.

Creamean, J. M., Suski, K. J., Rosenfeld, D., Cazorla, A., DeMott, P. J., Sullivan, R. C., White, A. B., Ralph, F. M., Minnis, P., Comstock, J. M., Tomlinson, J. M., and Prather, K. A.:

Dust and biological aerosols from the Sahara and Asia influence precipitation in the western U.S., Science, 339, 1572–1578, 2013.

Duce, R. A., LaRoche, J., Altieri, K., Arrigo, K. R., Baker, A. R., Capone, D. G., Cornell, S., Dentener, F., Galloway, J., Ganeshram, R. S., Geider, R. J., Jickells, T., Kuypers, M. M., Langlois, R., Liss, P. S., Liu, S. M., Middelburg, J. J., Moore, C. M., Nickovic, S., Oschlies, A., Pedersen, T., Prospero, J., Schlitzer, R., Seitzinger, S., Sorensen, L. L., Uematsu, M., Ulloa, O., Voss, M., Ward, B., and Zamora, L.: Impacts of atmospheric anthropogenic nitrogen on the open ocean, Science, 320, 893–897, doi:10.1126/science.1150369, 2008.

Fairlie, T. D., Jacob, D. J., Dibb, J. E., Alexander, B., Avery, M. A., van Donkelaar, A., and Zhang, L.: Impact of mineral dust on nitrate, sulfate, and ozone in transpacific Asian pollution plumes, Atmos. Chem. Phys., 10, 3999–4012, doi:10.5194/acp-10-3999-2010, 2010.

Finlayson-Pitts, B. J., Wingen, L. M., Sumner, A. L., Syomin, D., and Ramazan, K. A.: The heterogeneous hydrolysis of NO_2 in laboratory systems and in outdoor and indoor atmospheres: an integrated mechanism, Phys. Chem. Chem. Phys., 5, 223–242, 2003.

Formenti, P., Schütz, L., Balkanski, Y., Desboeufs, K., Ebert, M., Kandler, K., Petzold, A., Scheuvens, D., Weinbruch, S., and Zhang, D.: Recent progress in understanding physical and chemical properties of African and Asian mineral dust, Atmos. Chem. Phys., 11, 8231–8256, doi:10.5194/acp-11-8231-2011, 2011.

Geng, H., Hwang, H., Liu, X., Dong, S., and Ro, C.-U.: Investigation of aged aerosols in size-resolved Asian dust storm particles transported from Beijing, China, to Incheon, Korea, using low-*Z* particle EPMA, Atmos. Chem. Phys., 14, 3307–3323, doi:10.5194/acp-14-3307-2014, 2014.

Grassian, V. H.: Heterogeneous uptake and reaction of nitrogen oxides and volatile organic compounds on the surface of atmospheric particles including oxides, carbonates, soot and mineral dust: implications for the chemical balance of the troposphere, Int. Rev. Phys. Chem., 20, 467–548, 2001.

Hanisch, F. and Crowley, J. N.: The heterogeneous reactivity of gaseous nitric acid on authentic mineral dust samples, and on individual mineral and clay mineral components, Phys. Chem. Chem. Phys., 3, 2474–2482, 2001.

He, H.: Mineral dust and NO_x promote the conversion of SO_2 to sulfate in heavy pollution days, Scientific Reports, 4, 4172–4176, 2014.

Hinds, W. C.: Aerosol Technology: Properties, Behavior, and Measurement of Airborne Particles, John Willy & Sons, New York, 1999.

Huang, K., Zhuang, G., Li, J., Wang, Q., Sun, Y., Lin, Y., and Fu, J. S.: Mixing of Asian dust with pollution aerosol and the transformation of aerosol components during the dust storm over China in spring 2007, J. Geophys. Res.-Atmos., 115, D00K13, doi:10.1029/2009JD013145, 2010.

Huang, K., Zhuang, G., Wang, Q., Fu, J. S., Lin, Y., Liu, T., Han, L., and Deng, C.: Extreme haze pollution in Beijing during January 2013: chemical characteristics, formation mechanism and role of fog processing, Atmos. Chem. Phys. Discuss., 14, 7517–7556, doi:10.5194/acpd-14-7517-2014, 2014.

Huebert, B. J., Bates, T., Russell, P. B., Shi, G. Y., Kim, Y. J., Kawamura, K., Carmichael, G., and Nakajima, T.: An overview of ACE-Asia: strategies for quantifying the relationships between Asian aerosols and their climatic impacts, J. Geophys. Res.-Atmos., 108, 8663, doi:10.1029/2003JD003550, 2003.

Jickells, T. D., An, Z. S., Andersen, K. K., Baker, A. R., Bergametti, G., Brooks, N., Cao, J. J., Boyd, P. W., Duce, R. A., Hunter, K. A., Kawahata, H., Kubilay, N., laRoche, J., Liss, P. S., Mahowald, N., Prospero, J. M., Ridgwell, A. J., Tegen, I., and Torres, R.: Global iron connections between desert dust, ocean biogeochemistry, and climate, Science, 308, 67–71, 2005.

Kanakidou, M., Duce, R. A., Prospero, J. M., Baker, A. R., Benitez-Nelson, C., Dentener, F. J., Hunter, K. A., Liss, P. S., Mahowald, N., Okin, G. S., Sarin, M., Tsigaridis, K., Uematsu, M., Zamora, L. M., and Zhu, T.: Atmospheric fluxes of organic N and P to the global ocean, Global Biogeochem. Cy., 26, GB3026, doi:10.1029/2011GB004277, 2012.

Kim, Y. S., Iwasaka, Y., Shi, G. Y., Nagatani, T., Shibata, T., Trochkin, D., Matsuki, A., Yamada, M., Chen, B., Zhang, D., Nagatani, M., and Nakata, H.: Dust particles in the free atmosphere over desert areas on the Asian continent: measurements from summer 2001 to summer 2002 with balloon-borne optical particle counter and lidar, Dunhuang, China, J. Geophys. Res.-Atmos., 109, D19S26, doi:10.1029/2002JD003269, 2004.

Laskin, A., Wietsma, T. W., Krueger, B. J., and Grassian, V. H.: Heterogeneous chemistry of individual mineral dust particles with nitric acid: a combined CCSEM/EDX, ESEM, and ICP-MS study, J. Geophys. Res.-Atmos., 110, D10208, doi:10210.11029/12004JD005206, 2005.

Leaitch, W. R., Macdonald, A. M., Anlauf, K. G., Liu, P. S. K., Toom-Sauntry, D., Li, S.-M., Liggio, J., Hayden, K., Wasey, M. A., Russell, L. M., Takahama, S., Liu, S., van Donkelaar, A., Duck, T., Martin, R. V., Zhang, Q., Sun, Y., McKendry, I., Shantz, N. C., and Cubison, M.: Evidence for Asian dust effects from aerosol plume measurements during INTEX-B 2006 near Whistler, BC, Atmos. Chem. Phys., 9, 3523–3546, doi:10.5194/acp-9-3523-2009, 2009.

Li, G., Chen, J., Chen, Y., Yang, J., Ji, J., and Liu, L.: Dolomite as a tracer for the source regions of Asian dust, J. Geophys. Res.-Atmos., 112, D17201, doi:10.1029/2007JD008676, 2007.

Li, W. J. and Shao, L. Y.: Observation of nitrate coatings on atmospheric mineral dust particles, Atmos. Chem. Phys., 9, 1863–1871, doi:10.5194/acp-9-1863-2009, 2009.

Li, W., Shao, L., Shi, Z., Chen, J., Yang, L., Yuan, Q., Yan, C., Zhang, X., Wang, Y., Sun, J., Zhang, Y., Shen, X., Wang, Z., and Wang, W.: Mixing state and hygroscopicity of dust and haze particles before leaving Asian continent, J. Geophys. Res.-Atmos., 119, 1044–1059, 2014.

Lu, Z., Streets, D. G., Zhang, Q., Wang, S., Carmichael, G. R., Cheng, Y. F., Wei, C., Chin, M., Diehl, T., and Tan, Q.: Sulfur dioxide emissions in China and sulfur trends in East Asia since 2000, Atmos. Chem. Phys., 10, 6311–6331, doi:10.5194/acp-10-6311-2010, 2010.

Maher, B. A., Mutch, T. J., and Cunningham, D.: Magnetic and geochemical characteristics of Gobi Desert surface sediments: implications for provenance of the Chinese Loess Plateau, Geology, 37, 279–282, 2009.

Manktelow, P. T., Carslaw, K. S., Mann, G. W., and Spracklen, D. V.: The impact of dust on sulfate aerosol, CN and CCN during an East Asian dust storm, Atmos. Chem. Phys., 10, 365–382, doi:10.5194/acp-10-365-2010, 2010.

McNaughton, C. S., Clarke, A. D., Kapustin, V., Shinozuka, Y., Howell, S. G., Anderson, B. E., Winstead, E., Dibb, J., Scheuer, E., Cohen, R. C., Wooldridge, P., Perring, A., Huey, L. G., Kim, S., Jimenez, J. L., Dunlea, E. J., DeCarlo, P. F., Wennberg, P. O., Crounse, J. D., Weinheimer, A. J., and Flocke, F.: Observations of heterogeneous reactions between Asian pollution and mineral dust over the Eastern North Pacific during INTEX-B, Atmos. Chem. Phys., 9, 8283–8308, doi:10.5194/acp-9-8283-2009, 2009.

Menon, S., Unger, N., Koch, D., Francis, J., Garrett, T., Sednev, I., Shindell, D., and Streets, D.: Aerosol climate effects and air quality impacts from 1980 to 2030, Environ. Res. Lett., 3, 024004, doi:10.1088/1748-9326/3/2/024004, 2008.

Mochida, M., Umemoto, N., Kawamura, K., Lim, H., and Turpin, B. J.: Bimodal size distributions of various organic acids and fatty acids in the marine atmosphere: influence of anthropogenic aerosols, Asian dusts, and sea spray off the coast of East Asia, J. Geophys. Res., 112, D15209, doi:10.1029/2006JD007773, 2007.

Mogili, P. K., Kleiber, P. D., Young, M. A., and Grassian, V. H.: N_2O_5 hydrolysis on the components of mineral dust and sea salt aerosol: comparison study in an environmental aerosol reaction chamber, Atmos. Environ., 40, 7401–7408, 2006.

Nie, W., Wang, T., Xue, L. K., Ding, A. J., Wang, X. F., Gao, X. M., Xu, Z., Yu, Y. C., Yuan, C., Zhou, Z. S., Gao, R., Liu, X. H., Wang, Y., Fan, S. J., Poon, S., Zhang, Q. Z., and Wang, W. X.: Asian dust storm observed at a rural mountain site in southern China: chemical evolution and heterogeneous photochemistry, Atmos. Chem. Phys., 12, 11985–11995, doi:10.5194/acp-12-11985-2012, 2012.

Parrington, J. R., Zoller, W. H., and Aras, N. K.: Asian dust: seasonal transport to the Hawaiian Islands, Science, 220, 195–197, 1983.

Pathak, R. K., Wang, T., and Wu, W. S.: Nighttime enhancement of $PM_{2.5}$ nitrate in ammonia-poor atmospheric conditions in Beijing and Shanghai: plausible contributions of heterogeneous hydrolysis of N_2O_5 and HNO_3 partitioning, Atmos. Environ., 45, 1183–1191, 2011.

Saliba, N. A. and Chamseddine, A.: Uptake of acid pollutants by mineral dust and their effect on aerosol solubility, Atmos. Environ., 46, 256–263, 2012.

Seinfeld, J. H., Carmichael, G. R., Arimoto, R., Conant, W. C., Brechtel, F. J., Bates, T. A., Cahill, T. A., Clarke, A. D., Doherty, S. J., Flatau, P. J., Huebert, B. J., Kim, J., Markowicz, K. M., Quinn, P. K., Russell, L. M., Russell, P. B., Shimizu, A., Shinozuka, Y., Song, C. H., Tang, Y. H., Uno, I., Vogelmann, A. M., Weber, R. J., Woo, J. H., and Zhang, X. Y.: ACE-Asia: regional climatic and atmospheric chemical effects of Asian dust and pollution, B. Am. Meteorol. Soc., 85, 367–380, doi:10.1175/BAMS-85-3-367, 2004.

Singh, H. B., Brune, W. H., Crawford, J. H., Flocke, F., and Jacob, D. J.: Chemistry and transport of pollution over the Gulf of Mexico and the Pacific: spring 2006 INTEX-B campaign overview and first results, Atmos. Chem. Phys., 9, 2301–2318, doi:10.5194/acp-9-2301-2009, 2009.

Song, Y.-C., Eom, H.-J., Jung, H.-J., Malek, M. A., Kim, H. K., Geng, H., and Ro, C.-U.: Investigation of aged Asian dust particles by the combined use of quantitative ED-EPMA and ATR-FTIR imaging, Atmos. Chem. Phys., 13, 3463–3480, doi:10.5194/acp-13-3463-2013, 2013.

Sullivan, R. C. and Prather, K. A.: Investigations of the diurnal cycle and mixing state of oxalic acid in individual particles in Asian aerosol outflow, Environ. Sci. Technol., 41, 8062–8069, 2007.

Sullivan, R. C., Guazzotti, S. A., Sodeman, D. A., and Prather, K. A.: Direct observations of the atmospheric processing of Asian mineral dust, Atmos. Chem. Phys., 7, 1213–1236, doi:10.5194/acp-7-1213-2007, 2007.

Sullivan, R. C., Moore, M. J. K., Petters, M. D., Kreidenweis, S. M., Roberts, G. C., and Prather, K. A.: Effect of chemical mixing state on the hygroscopicity and cloud nucleation properties of calcium mineral dust particles, Atmos. Chem. Phys., 9, 3303–3316, doi:10.5194/acp-9-3303-2009, 2009a.

Sullivan, R. C., Moore, M. J. K., Petters, M. D., Kreidenweis, S. M., Roberts, G. C., and Prather, K. A.: Timescale for hygroscopic conversion of calcite mineral particles through heterogeneous reaction with nitric acid, Phys. Chem. Chem. Phys., 11, 7826–7837, 2009b.

Sun, Y., Zhuang, G., Huang, K., Li, J., Wang, Q., Wang, Y., Lin, Y., Fu, J. S., Zhang, W., Tang, A., and Zhao, X.: Asian dust over northern China and its impact on the downstream aerosol chemistry in 2004, J. Geophys. Res., 115, D00K09, doi:10.1029/2009jd012757, 2010.

Takahashi, Y., Higashi, M., Furukawa, T., and Mitsunobu, S.: Change of iron species and iron solubility in Asian dust during the long-range transport from western China to Japan, Atmos. Chem. Phys., 11, 11237–11252, doi:10.5194/acp-11-11237-2011, 2011.

Tobo, Y., Zhang, D., Matsuki, A., and Iwasaka, Y.: Asian dust particles converted into aqueous droplets under remote marine atmospheric conditions, P. Natl. Acad. Sci. USA, 107, 17905–17910, 2010.

Uno, I., Eguchi, K., Yumimoto, K., Takemura, T., Shimizu, A., Uematsu, M., Liu, Z. Y., Wang, Z. F., Hara, Y., and Sugimoto, N.: Asian dust transported one full circuit around the globe, Nat. Geosci., 2, 557–560, 2009.

Usher, C. R., Michel, A. E., and Grassian, V. H.: Reactions on mineral dust, Chem. Rev., 103, 4883–4939, 2003.

van Donkelaar, A., Martin, R. V., Brauer, M., Kahn, R., Levy, R., Verduzco, C., and Villeneuve, P. J.: Global estimates of ambient fine particulate matter concentrations from satellite-based aerosol optical depth: development and application, Environ. Health Persp., 118, 8347–8355, 2010.

Wang, G., Xie, M., Hu, S., Gao, S., Tachibana, E., and Kawamura, K.: Dicarboxylic acids, metals and isotopic compositions of C and N in atmospheric aerosols from inland China: implications for dust and coal burning emission and secondary aerosol formation, Atmos. Chem. Phys., 10, 6087–6096, doi:10.5194/acp-10-6087-2010, 2010.

Wang, G., Li, J., Cheng, C., Hu, S., Xie, M., Gao, S., Zhou, B., Dai, W., Cao, J., and An, Z.: Observation of atmospheric aerosols at Mt. Hua and Mt. Tai in central and east China during spring 2009 – Part 1: EC, OC and inorganic ions, Atmos. Chem. Phys., 11, 4221–4235, doi:10.5194/acp-11-4221-2011, 2011.

Wang, G. H., Li, J. J., Cheng, C. L., Zhou, B. H., Xie, M. J., Hu, S. Y., Meng, J. J., Sun, T., Ren, Y. Q., Cao, J. J., Liu, S. X., Zhang, T., and Zhao, Z. Z.: Observation of atmospheric aerosols at Mt. Hua and Mt. Tai in central and east China during spring 2009 – Part 2: Impact of dust storm on organic aerosol composition and size distribution, Atmos. Chem. Phys., 12, 4065–4080, doi:10.5194/acp-12-4065-2012, 2012.

Wang, G. H., Zhou, B. H., Cheng, C. L., Cao, J. J., Li, J. J., Meng, J. J., Tao, J., Zhang, R. J., and Fu, P. Q.: Impact of Gobi desert dust on aerosol chemistry of Xi'an, inland China during spring 2009: differences in composition and size distribution between the urban ground surface and the mountain atmosphere, Atmos. Chem. Phys., 13, 819–835, doi:10.5194/acp-13-819-2013, 2013.

Wang, S. W., Zhang, Q., Streets, D. G., He, K. B., Martin, R. V., Lamsal, L. N., Chen, D., Lei, Y., and Lu, Z.: Growth in NO_x emissions from power plants in China: bottom-up estimates and satellite observations, Atmos. Chem. Phys., 12, 4429–4447, doi:10.5194/acp-12-4429-2012, 2012.

Wang, Y., Zhang, Q. Q., He, K., Zhang, Q., and Chai, L.: Sulfate-nitrate-ammonium aerosols over China: response to 2000–2015 emission changes of sulfur dioxide, nitrogen oxides, and ammonia, Atmos. Chem. Phys., 13, 2635–2652, doi:10.5194/acp-13-2635-2013, 2013.

Wang, Y. H., Hu, B., Ji, D. S., Liu, Z. R., Tang, G. Q., Xin, J. Y., Zhang, H. X., Song, T., Wang, L. L., Gao, W. K., Wang, X. K., and Wang, Y. S.: Ozone weekend effects in the Beijing–Tianjin–Hebei metropolitan area, China, Atmos. Chem. Phys., 14, 2419–2429, doi:10.5194/acp-14-2419-2014, 2014.

Wu, F., Zhang, D., Cao, J., Xu, H., and An, Z.: Soil-derived sulfate in atmospheric dust particles at Taklimakan desert, Geophys. Res. Lett., 39, L24803, doi:10.1029/2012GL054406, 2012.

Zamora, L. M., Prospero, J. M., and Hansell, D. A.: Organic nitrogen in aerosols and precipitation at Barbados and Miami: implications regarding sources, transport and deposition to the western subtropical North Atlantic, J. Geophys. Res., 116, D20309, doi:10.1029/2011JD015660, 2011.

Zamora, L. M., Prospero, J. M., Hansell, D. A., and Trapp, J. M.: Atmospheric P deposition to the subtropical North Atlantic: sources, properties, and relationship to N deposition, J. Geophys. Res.-Atmos., 118, 1546–1562, doi:10.1002/jgrd.50187, 2013.

Zhang, Q., Streets, D. G., Carmichael, G. R., He, K. B., Huo, H., Kannari, A., Klimont, Z., Park, I. S., Reddy, S., Fu, J. S., Chen, D., Duan, L., Lei, Y., Wang, L. T., and Yao, Z. L.: Asian emissions in 2006 for the NASA INTEX-B mission, Atmos. Chem. Phys., 9, 5131–5153, doi:10.5194/acp-9-5131-2009, 2009.

Zheng, X.: Salt lakes on the Inner Mongolian plateau of China, Chinese Geographic Science, 1, 83–94, 1991.

Table 1. Meteorological parameters and hourly concentrations of inorganic ions, elements, EC, OC, water-soluble organic (WSOC) and inorganic carbon(WSIC) and water-soluble organic (WSON) and inorganic nitrogen (WSIN) in total suspended particles (TSP) during the dust storm, transition and non-dust periods.

Time	Dust storm (9 Mar, 18:00–10 Mar, 21:00 LT)	Transition (10 Mar, 21:00–11 Mar, 12:00 LT)	Non-dust storm (11 Mar, 12:00–12 Mar, 10:00 LT)
I. Meteorological parameters and online measured $PM_{2.5}$			
Relative humidity (RH, %)	22 ± 3.5 (14–26)	53 ± 9.0 (34–64)	48 ±6.0 (33–61)
Wind speed (WS, $m\,s^{-1}$)	2.0 ± 0.6 (0.7–2.9)	1.6 ± 0.7 (0.7–3.5)	2.1 ± 0.8 (0.4–3.2)
Temperature (T, °C)	13 ± 2.7 (9.1–20)	5.4 ± 1.7 (3.3–8.5)	10 ± 1.3 (8.8–15)
$PM_{2.5}$, $\mu g\,m^{-3}$	152 ± 127 (49–621)	88 ± 16 (68–125)	150 ± 32 (119–279)
II. Inorganic ions in TSP samples, $\mu g\,m^{-3}$			
F^-	0.5 ± 0.4 (0.1–1.3)	0.6 ± 0.3 (0.2–1.3)	0.8 ± 0.2 (0.3–1.0)
Cl^-	5.1 ± 6.3 (1.7–34)	2.8 ± 0.8 (1.7–4.9)	4.3 ± 2.0 (1.9–11)
NO_2^-	0.3 ± 0.2 (0.0–0.7)	0.3 ± 0.1 (0.0–0.4)	0.2 ± 0.1 (0.0–0.3)
NO_3^-	8.2 ± 2.1 (4.7–12)	11 ± 2.0 (7.6–15)	28 ± 3.5 (20–34)
SO_4^{2-}	35 ± 34 (12–180)	14 ± 3.3 (10–20)	21 ± 4.3 (15–33)
Na^+	18 ± 13 (5.2–72)	8.7 ± 1.5 (5.4–11)	3.9 ± 4.1 (0.0–13)
NH_4^+	3.0 ± 0.7 (1.7–5.1)	3.5 ± 1.0 (2.4–5.9)	7.6 ± 0.9 (5.6–8.7)
K^+	1.5 ± 0.8 (0.7–4.1)	0.8 ± 0.2 (0.4–1.2)	1.4 ± 0.5 (0.9–3.0)
Mg^{2+}	1.3 ± 0.7 (0.3–3.8)	0.7 ± 0.2 (0.3–1.1)	0.7 ± 0.3 (0.3–1.4)
Ca^{2+}	10 ± 5.9 (1.7–28)	6.6 ± 1.9 (2.8–9.8)	11 ± 2.5 (6.9–15)
Subtotal	83 ± 60 (37–340)	49 ± 8.4 (36–65)	79 ± 10 (56–103)
III. Elements in TSP samples, $\mu g\,m^{-3}$			
S	18 ± 11 (7.9–56)	7.9 ± 1.9 (5.7–12)	13 ± 2.2 (9.3–19)
Cl	6.2 ± 6.0 (2.0–30)	2.5 ± 1.3 (1.5–6.4)	6.6 ± 2.4 (3.9–12)
K	64 ± 39 (28–195)	15 ± 4.2 (9.0–21)	20 ± 4.6 (13–33)
Ca	146 ± 81 (66–411)	45 ± 15 (26–71)	55 ± 13 (35–98)
Ti	9.7 ± 6.0 (4.3–30)	2.4 ± 0.7 (1.4–3.4)	2.5 ± 0.6 (1.8–4.8)
Mn	1.2 ± 1.0 (0.0–4.3)	0.5 ± 0.7 (0.0–2.3)	0.4 ± 0.8 (0.0–3.9)
Fe	109 ± 69 (45–346)	25 ± 8.2 (15–38)	26 ± 7.5 (15–52)
Zn	0.7 ± 0.3 (0.4–1.5)	0.9 ± 0.6 (0.4–2.6)	1.4 ± 1.1 (0.6–4.1)
Cr	0.22 ± 0.12 (0.10–0.65)	0.09 ± 0.04 (0.00–0.18)	0.10 ± 0.03 (0.03–0.16)
Ni	0.04 ± 0.04 (0.00–0.14)	0.04 ± 0.02 (0.00–0.07)	0.04 ± 0.03 (0.00–0.10)
As	0.03 ± 0.05 (0.00–0.23)	0.01 ± 0.02 (0.00–0.07)	0.04 ± 0.07 (0.00–0.27)
Br	0.00 ± 0.00 (0.00–0.02)	0.02 ± 0.03 (0.00–0.11)	0.030 ± 0.04 (0.00–0.15)
Mo	0.04 ± 0.05 (0.00–0.17)	0.04 ± 0.06 (0.00–0.19)	0.04 ± 0.08 (0.00–0.26)
Pb	0.37 ± 0.19 (0.09–0.77)	0.39 ± 0.15 (0.20–0.71)	0.39 ± 0.12 (0.14–0.65)
Subtotal[a]	506 ± 304 (193–1559)	148 ± 42 (92–225)	191 ± 43 (136–335)
IV. Other species in TSP samples, $\mu g\,m^{-3}$			
WSOC	15 ± 10 (4.2–52)	15 ± 17 (2.0–58)	19 ± 11 (7.8–49)
WSIC	10 ± 2.8 (6.8–20)	5.9 ± 3.3 (1.9–13)	6.0 ± 1.7 (2.9–9.5)
WSIN	4.2 ± 1.0 (2.4–6.5)	5.2 ± 1.2 (3.6–8.0)	12 ± 1.3 (9.1–14)
WSON	2.5 ± 1.8 (0.0–8.0)	1.7 ± 0.8 (0.5–3.1)	5.9 ± 3.6 (1.4–16)
OC	68 ± 50 (8.7–254)	32 ± 9.1 (20–49)	55 ± 13 (37–84)
EC	6.7 ± 8.6 (0.0–3.2)	7.1 ± 2.4 (3.4–12)	8.9 ± 6.2 (0.0–28)
TSP	2109 ± 1360 (774–7527)	630 ± 155 (412–1037)	687 ± 194 (476–1399)
$PM_{2.5}$/TSP, %	7.4 ± 3.4 (2.3–13)	14 ± 2.4 (9.6–18)	23 ± 4.8 (10–30)

[a] Calculated as SO_4^{2-} + Cl^- + metal oxides.

Table 2. Accumulative percentages (%) of mass concentrations of major ions on the 9-stage filters collected in Xi'an during the spring dust storm and non-dust storm periods.

Size range, µm	Cl^-	NO_3^-	SO_4^{2-}	NH_4^+	Na^+	K^+	Mg^{2+}	Ca^{2+}
Dust storm period (9 Mar, 18:00–10 Mar, 21:00 LT)								
> 9.0	100	100	100	100	100	100	100	100
5.8–9.0	86 ± 1	87 ± 1	83 ± 3	74 ± 10	87 ± 1	88 ± 5	85 ± 2	83 ± 6
4.7–5.8	74 ± 2	71 ± 4	64 ± 5	52 ± 9	75 ± 2	69 ± 3	70 ± 3	68 ± 5
3.3–4.7	62 ± 2	60 ± 5	51 ± 5	37 ± 17	62 ± 3	62 ± 9	57 ± 2	49 ± 7
2.1–3.3	51 ± 2	44 ± 6	37 ± 7	31 ± 13	51 ± 3	49 ± 9	43 ± 3	32 ± 6
1.1–2.1	40 ± 4	31 ± 6	27 ± 7	21 ± 16	39 ± 4	40 ± 7	31 ± 3	18 ± 5
0.7–1.1	31 ± 4	22 ± 5	20 ± 6	18 ± 12	28 ± 3	29 ± 5	22 ± 3	10 ± 4
0.4–0.7	21 ± 2	17 ± 2	14 ± 4	16 ± 8	19 ± 3	24 ± 0	14 ± 3	5 ± 4
< 0.4	11 ± 1	9 ± 1	7 ± 2	9 ± 5	9 ± 1	11 ± 1	7 ± 2	2 ± 2
Non-dust storm period (11 Mar, 12:00–12 Mar, 21:00 LT)								
> 9.0	100	100	100	100	100	100	100	100
5.8–9.0	84	80	86	77	90	93	88	91
4.7–5.8	77	75	76	73	80	86	74	77
3.3–4.7	70	70	69	72	69	80	63	64
2.1–3.3	62	64	62	69	58	74	50	48
1.1–2.1	55	58	54	65	46	66	39	35
0.7–1.1	42	42	40	46	35	46	29	25
0.4–0.7	29	25	28	27	24	28	23	22
< 0.4	16	3	15	1	13	9	17	19

Title Page
Abstract Introduction
Conclusions References
Tables Figures
◀| |▶
◀ ▶
Back Close
Full Screen / Esc
Printer-friendly Version
Interactive Discussion

Table 3. Concentrations (µg m^{-3}) of different sulfates in the water-soluble fraction of TSP samples and their relative abundances (%) to the total water-soluble sulfate during the dust storm and transition periods.

		K_2SO_4	$MgSO_4$	Na_2SO_4	$CaSO_4$
Dust storm period	Concentration	3.4 ± 1.7 (1.6–9.2)	13 ± 7.1 (3.3–38)	45 ± 30 (11–155)	35 ± 20 (5.8–95)
	Relative abundance	3.6 ± 0.7 (2.5–4.7)	13 ± 2.6 (7.0–17)	47 ± 15 (21–77)	36 ± 12 (12–58)
Transition period	Concentration	1.9 ± 0.5 (0.8–2.8)	7.2 ± 2.0 (3.3–11)	21 ± 4.0 (12–25)	23 ± 6.5 (10–33)
	Relative abundance	3.0 ± 0.8 (2–5)	13 ± 1.8 (9–16)	41 ± 9.0 (26–64)	42 ± 7.6 (25–56)

(a) Dust storm period (Phase I) (b) Dust storm period (Phase I)

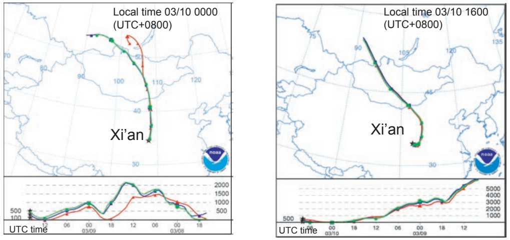

(c) Transition period (Phase II) (d) Non-dust storm period (Phase III)

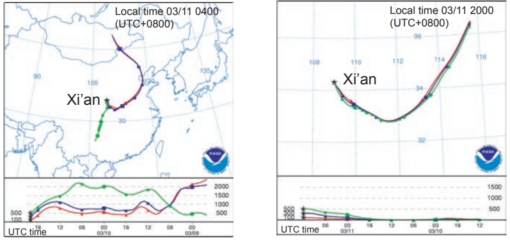

(e) Topography of Ganzhong Basin and it's surrounding areas

Phase I: Dust storm period (03/09,1800-03/10,2100),
Phase II: Transition period (03/10,2200-03/11,1200),
Phase III: Non-dust storm period (03/11,1200-03/12,1000)

Figure 1. Backward trajectories of air masses arriving in Xi'an during the campaign **(a–d)** and the topography of Guanzong Basin and it's surrounding areas **(e)** (duration 48 h, air parcels of 100, 300 and 500 m above ground level are in red, blue and green).

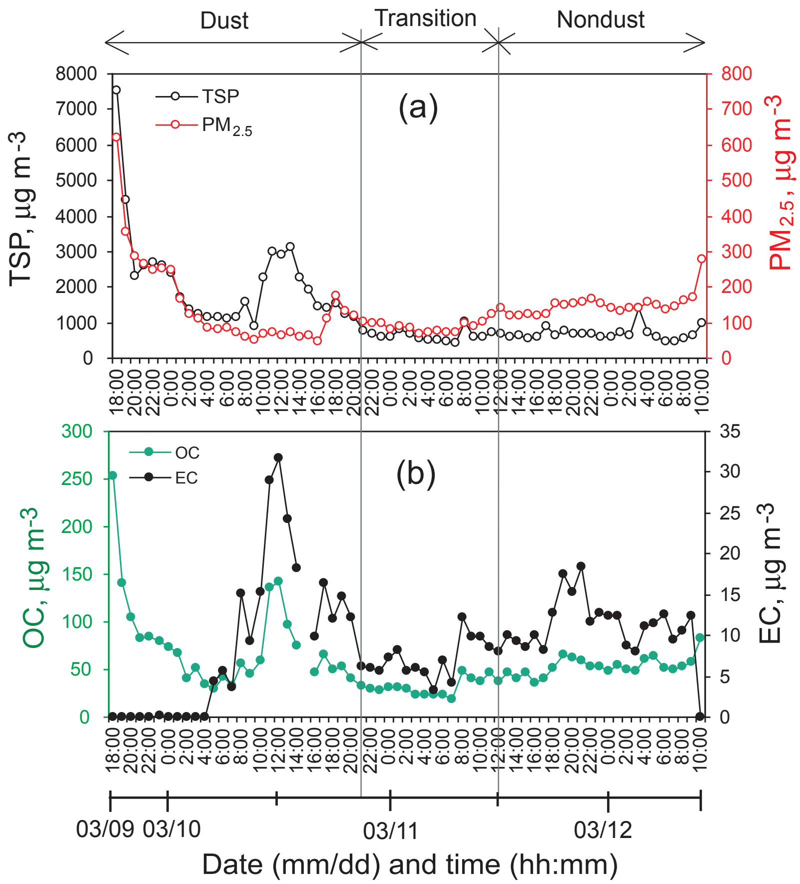

Figure 2. Temporal variations of TSP, $PM_{2.5}$, EC and OC during the campaign.

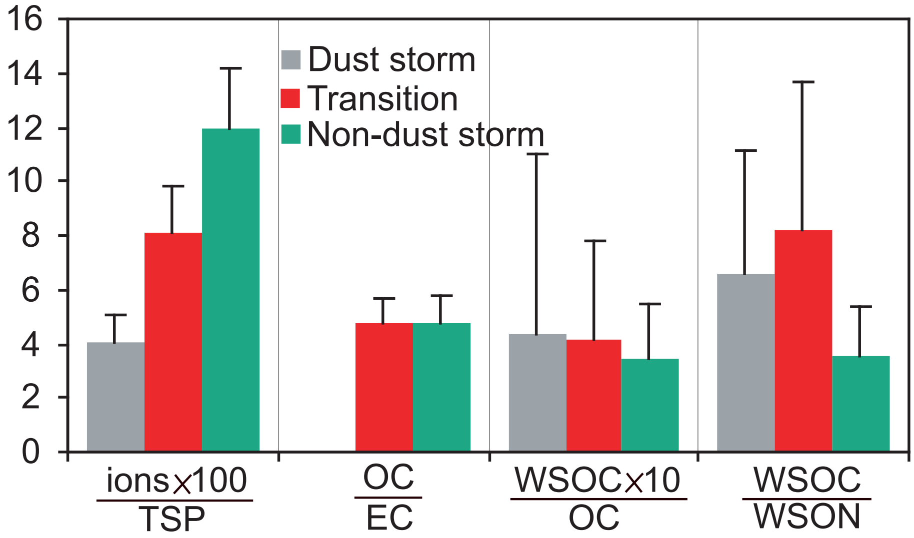

Figure 3. Comparison of relative abundance of ions, OC, EC, WSOC and WSON in the TSP samples during the dust storm event, transition time and non-dust storm period.

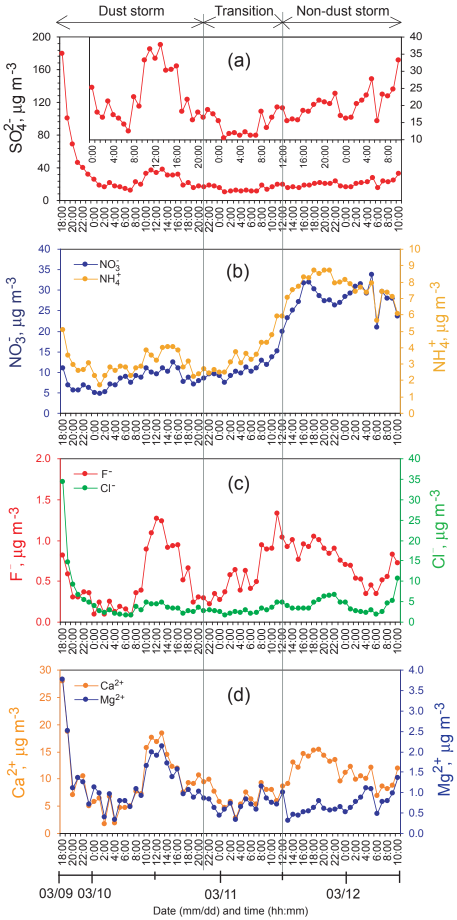

Figure 4. Temporal variations of inorganic ions during the campaign.

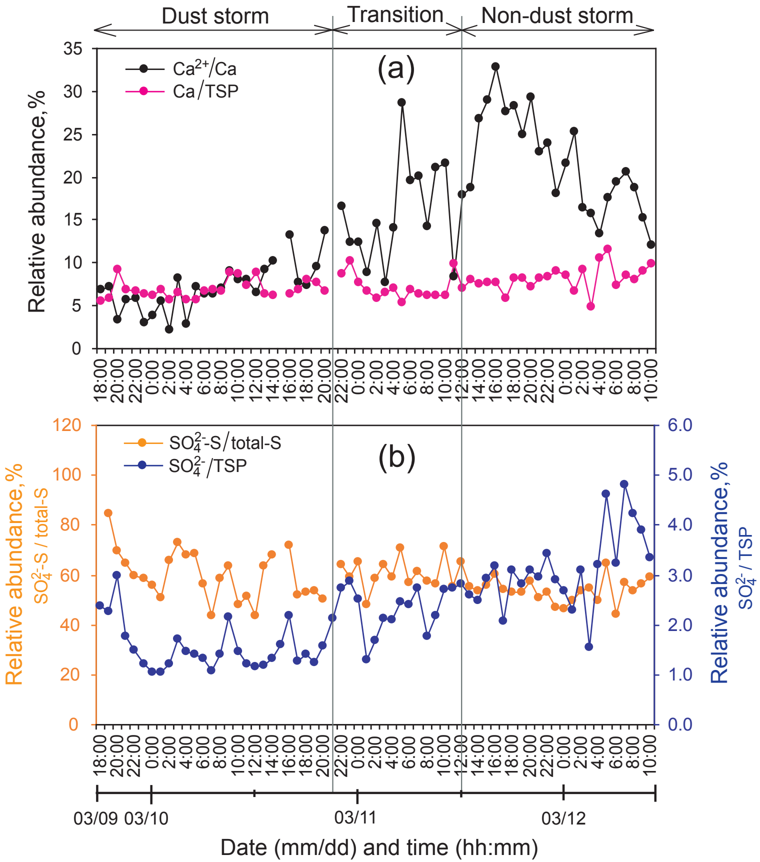

Figure 5. Relative abundances of Ca^{2+}/Ca, Ca/TSP, SO$_4^{2-}$-S/total-S and SO$_4^{2-}$/TSP during the campaign.

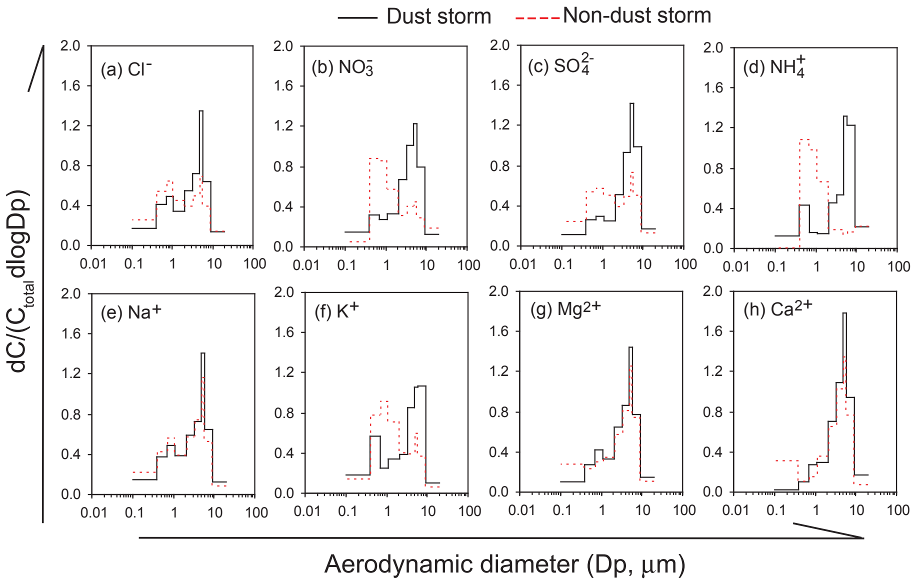

Figure 6. Size distributions of major ions during the dust and non-dust storm periods.

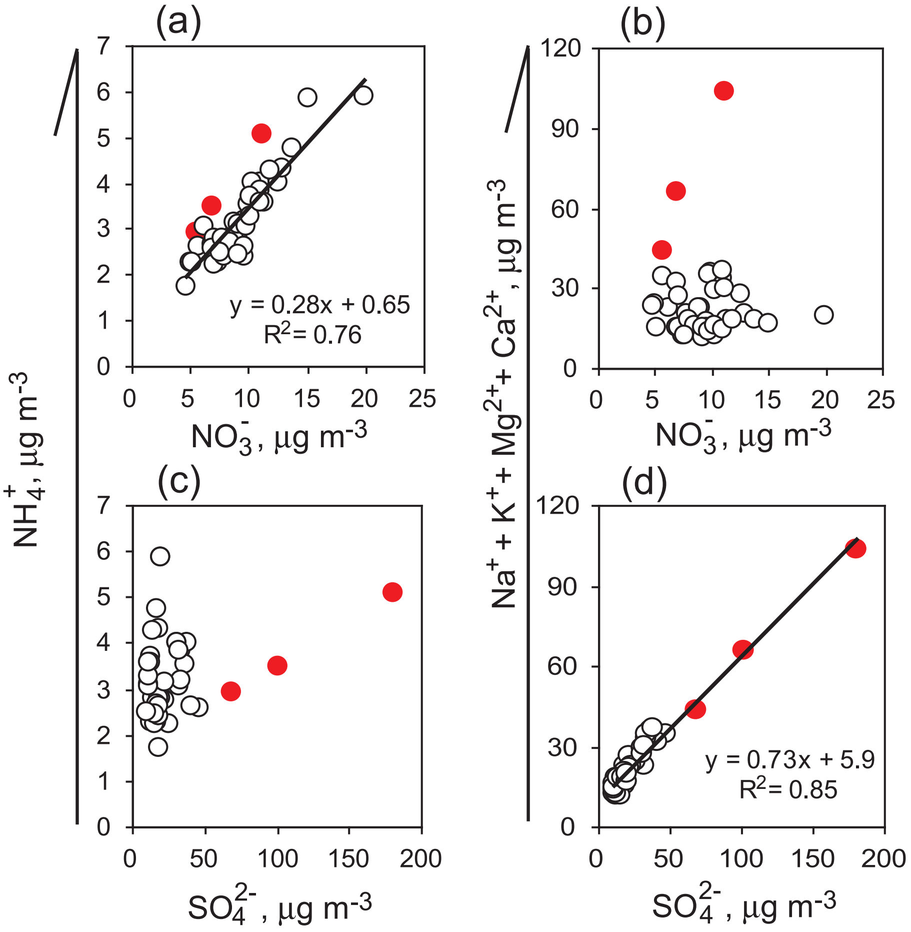

Figure 7. Linear fit regressions for nitrate and sulfate with ammonium and other cations in the TSP samples collected during the dust storm and transition periods (red dots are the three samples collected at the earliest three hours).

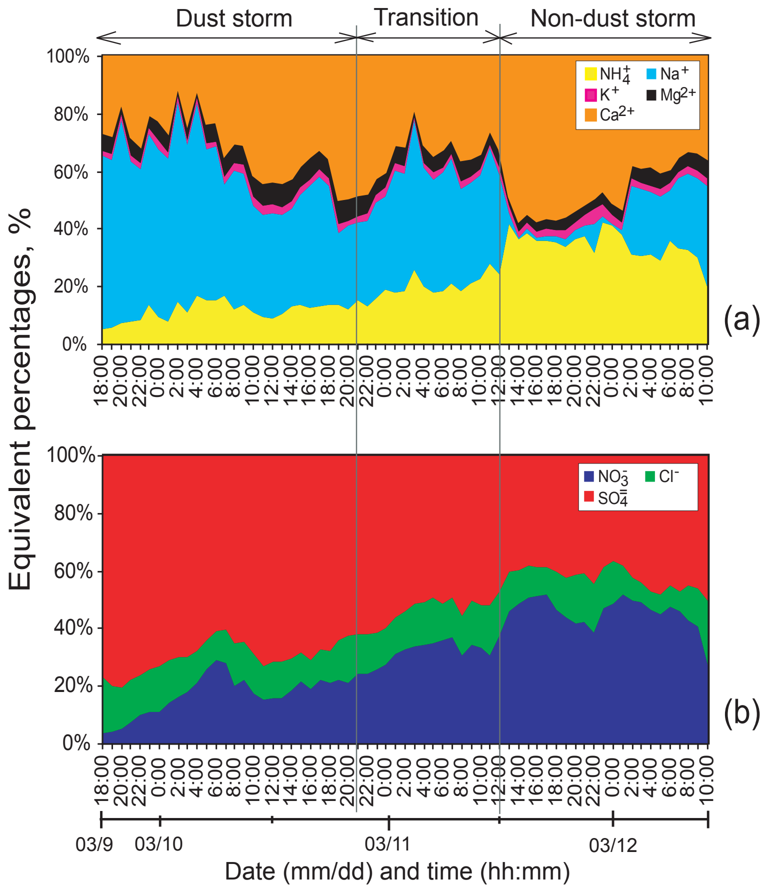

Figure 8. Equivalent percentages of inorganic ions in the TSP samples during the campaign.

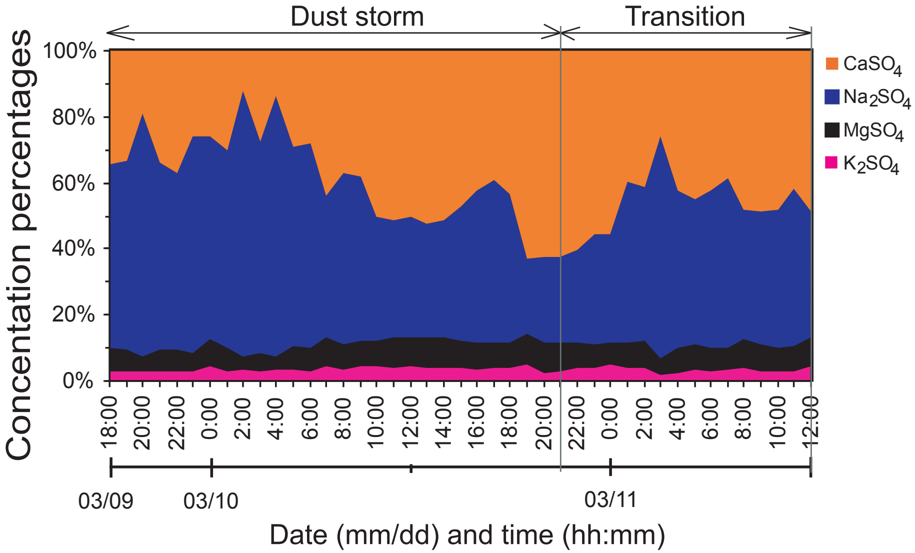

Figure 9. Chemical forms of water-soluble sulfate salts in the TSP samples during the dust storm and transition periods.

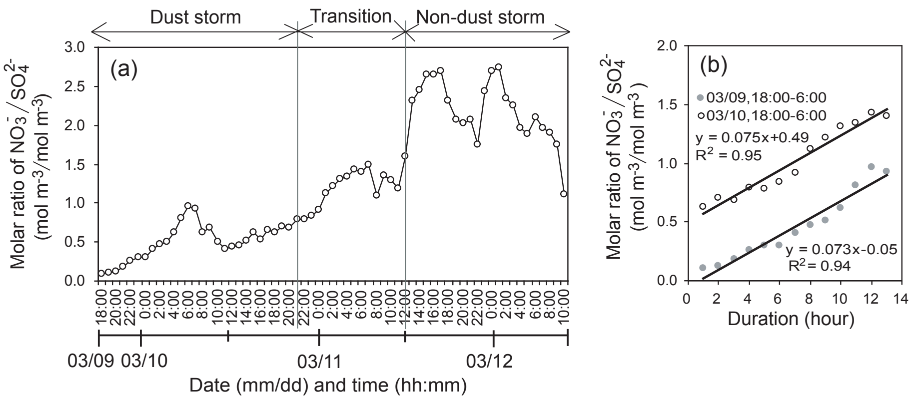

Figure 10. Production speed of nitrate during the sampling period **(a)** molar ratio of nitrate/sulfate in the TSP samples and **(b)** linear fit regression for the nighttime molar ratio of nitrate/sulfate with observation duration).

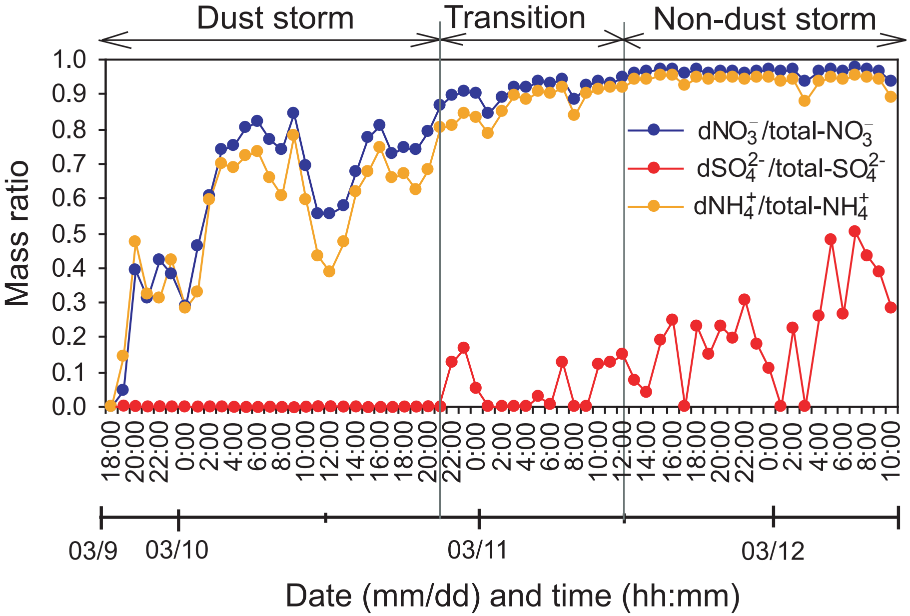

Figure 11. Mass ratios of nitrate, sulfate and ammonium produced by heterogeneous reactions to the totals in the TSP samples.

Title Page

Abstract | Introduction

Conclusions | References

Tables | Figures

◀| |▶

◀ ▶

Back | Close

Full Screen / Esc

Printer-friendly Version

Interactive Discussion

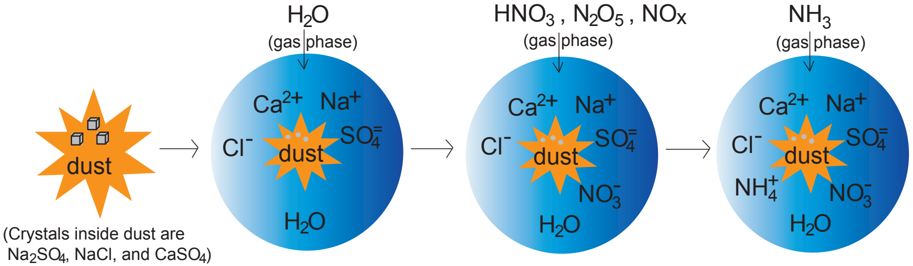

Figure 12. A diagram for heterogeneous formation mechanism of ammonium nitrate on dust surface in Xi'an during the dust storm event.